Gondwana Research 19 (2011) 994–1007

Contents lists available at ScienceDirect

Gondwana Research

journal homepage: www.elsevier.com/locate/gr

Crustal structure of the Paleozoic Kunlun orogeny from an active-source seismic profile between Moba and Guide in East Tibet, China

Zhongjie Zhang [a,*], Simon Klemperer [b], Zhiming Bai [a], Yun Chen [a], Jiwen Teng [a]

[a] State Key Laboratory of Lithospheric Evolution, Institute of Geology and Geophysics, Chinese Academy of Sciences, 100029 Beijing, PR China
[b] Department of Geophysics, Stanford University, Stanford, CA 94305, USA

ARTICLE INFO

Article history:
Received 5 July 2010
Received in revised form 23 September 2010
Accepted 24 September 2010
Available online 19 October 2010

Editor: W.J. Xiao

Keywords:
Eastern Kunlun mountains
Animaqing suture
Kunlun fault
Crustal structure
Wide-angle seismic profiling
Continental arc crust
Tibet Plateau

ABSTRACT

We herein present a new seismic refraction/wide-angle reflection profile that crosses the Songpan–Ganzi terrane, the Animaqing suture zone and the eastern Kunlun mountains (comprised of the South Kunlun and Middle Kunlun blocks separated by the Middle Kunlun fault). The profile is 380 km long and extends from Moba to Guide in eastern Tibet. The crustal thickness is about 62 km under the Songpan–Ganzi terrane, 62–64 km under the South Kunlun, and 60 km under the Middle Kunlun block. The Songpan–Ganzi flysch seems to be present up to a depth of 15 km south of the Animaqing suture zone, and up to a depth of 10 km in the Middle Kunlun block, with thicknesses elsewhere that depend on assumptions about the likely lithologies. The profile exhibits clear lateral variations both in the upper and lower crust, which are indicative of different crustal blocks juxtaposed by the Kunlun fault system. Whether or not the Songpan–Ganzi flysch was originally deposited on oceanic crust, at the longitude of our profile (100°E) it is now underlain by continental crust, and the presence of continental crust beneath the Songpan–Ganzi terrane and of a continental arc under the South Kunlun block suggest Paleozoic continent–continent arc collision in the eastern Kunlun Mountains. Comparison of crustal velocity columns from all wide-angle seismic profiles across the eastern Kunlun mountains indicates a remarkable west-to-east change in the Moho topography across the Kunlun fault system (15–20 km Moho step at 95°E, but only 2–5 km along our profile at 100°E). Lower-crustal thickness of the Kunlun terranes is rather uniform, about 35 km, from 80°–95°E, which suggests that similar thrust-thickening processes have played a role where the Qaidam Basin abuts the Kunlun fault, but thins to 20–25 km at 100°E, east of the Qaidam Basin. The increased crustal thickness from 93° to 98°E compared to that at 100°E may be due to the differences in the thickness of the crust of the two plates before their collision, and/or largely achieved by thickening of the lower crust, perhaps indicating a crustal flow mechanism operating more strongly in the western region.

1. Introduction

The formation of the Tibetan plateau is generally attributed to a series of complex accretionary collision events (Molnar et al., 1993; Owens and Zandt, 1997; Tapponnier et al., 2001; Chung et al., 2005; Dai et al., 2010). The geodynamic mechanism by which large plateaus are formed is of great interest to earth scientists. For Tibet, the mechanism may be characterized by several models of the collision between India and Eurasia. One fundamental area of disagreement in northern Tibet relates to whether multiple lithospheric slabs only subducted beneath the region from the south or whether there is or was also subduction from the north. In the uni-directional under-thrust model, Indian lithosphere subducts and/or Songpan–Ganzi oceanic lithosphere was subducted northwards beneath the Kunlun blocks (Powell and Conaghan, 1975; Molnar et al., 1993; Yin and Harrison, 2000) and the Qaidam basin to the north acts as an obstacle (Zhao and Morgan, 1985; Yin and Harrison, 2000). In the two-directional subduction model, in addition to this northward subduction, the Tarim basin and Qaidam basin lithosphere are (or were until recently) being subducted southwards (Xu et al., 1992; Deng, 1997; Arnaud et al., 1992; Pearce and Mei, 1988; Tapponnier et al., 2001; Kind et al., 2002; Zhang et al., 2010a,b,c). In many models, the deformation of the Tibetan Plateau sweeps progressively northwards, with deformation at the northern edge of Tibet occurring later than the India–Asia collision, and the Qaidam Basin today possibly being in the initial stages of plateau building (Metivier et al., 1998; Meyer et al., 1998; Chen et al., 1999; Tapponnier et al., 1990, 2001; Pares et al., 2003; Metcalfe, 2010).

Because of the controversy over the northern margin of Tibet, better knowledge of the crustal structure of the eastern Kunlun mountains along the northeastern boundary of the Tibetan plateau could have a significant impact on geodynamic models of the Indian–Asian collision and Tibetan plateau formation. Although a number of active and passive source seismic surveys have been carried out in the

* Corresponding author.
E-mail address: zhangzj@mail.iggcas.ac.cn (Z. Zhang).

1342-937X/$ – see front matter
doi:10.1016/j.gr.2010.09.008

northeastern Tibetan plateau over the last 10 years (Yuan and hua, 1996; Vergne et al., 2002; Galvé et al., 2002; Zhang et al., 2003; Liu et al., 2006; Zhao et al., 2008; Wang et al., in press; Zhang et al., 2010a), the large shot and receiver intervals that are used in most of the seismic acquisition programs described can only provide a first-order estimate of the characteristics of the crustal structure. In eastern Tibet, very complicated patterns of fault systems have developed over the course of multiple orogenic events. For example, the active Kunlun fault system formed along the Animaqing–Kunlun–Muztagh suture (AKMS) that is related to the late Paleozoic–Mesozoic accretion of the Kunlun Block to Gondwana. Many of the earlier deep geophysical studies adopted a simplified approach in treating the Kunlun fault system as one fault; hence, more detailed studies of crustal structure in east Tibet can be of benefit to our understanding of crustal deformation and plateau growth mechanisms.

2. Tectonic setting

Our deep seismic survey line crosses the Songpan–Ganzi terrane, and the South and Middle Kunlun blocks that also includes Songpan–Ganzi age turbidites, and passes eastward into the West Qinling terrane. To the north is the Qilian block, and beyond that the North China craton (Fig. 1). The Songpan–Ganzi terrane and the Kunlun blocks are separated by the Animaqing –Kunlun–Muztagh suture (AKMS) (faults F5–F6 on the lower panel of Fig. 1). The South and Middle Kunlun blocks are separated by the Middle (or sometimes Central) Kunlun fault (Fault F10 on the lower panel of Fig. 1), sometimes also called the central Kunlun fault (Jiang et al., 2000).

The Songpan–Ganzi block is a triangular tectonic unit that lies between the Kunlun blocks in the north, the Qiangtang Block in the south and Sichuan basin in the east (Zhang et al., 2010a,b,c). The characteristic Songpan–Ganzi Triassic turbidites, which are typically >10 km thick, are associated with the evolution of the Kunlun block in far-western Tibet, but with the collision of the North and South China cratons in the east, with these separate depocenters being amalgamated by a shortening associated with the collision of the Qiangtang Block with Eurasia (Weislogel, 2008). The closure of a Songpan–Ganzi remnant ocean during the Triassic to early Jurassic partially subducted the Songpan–Ganzi terrane beneath the Kunlun arc terrane along the AKMS (Burchfiel et al., 1989; Yin and Harrison, 2000). The eastern boundary of the Songpan–Ganzi terrane lies along the eastern edge of the southeast-directed, late Triassic/early Jurassic Longmenshan thrust belt that lies along the western edge of the South China (Yangtze) craton (Burchfiel et al., 1995; Fu et al., 2010; Zhang et al., 2009, Zhang et al., 2010a,b,c). Triassic strata conformably overlie the Paleozoic shallow marine sequences of South China (Burchfiel et al., 1995), which suggests that this is a slope-shelf transition that overlies a continental basement, at least in the easternmost part of the Songpan–Ganzi terrane (Yin and Harrison, 2000). It has been argued that continental crust floors the entire Songpan–Ganzi terrane, so that the entire flysch basin may represent a series of allochthons (Zhang, 2001).

The >1000 km-long East Kunlun fault system, which follows the trace of the AKMS, is an important WNW-trending boundary fault that lies close to the northern margin of the highest part of the Qinghai–Tibet Plateau (upper panel of Fig. 1). The AKMS represents a complex history of suturing of the Kunlun terranes to each other in the Late Proterozoic and Paleozoic, and collectively to the Songpan–Gangzi terrane during the Triassic (Yang et al., 1996). The East Kunlun fault system only became active as a strike-slip system during the last 7 Ma, with a total slip of 75 km (Fu and Awata, 2007) and a late Quaternary slip rate of 12±3 mm/yr (van der Woerd et al., 2000). The Middle Kunlun and South Kunlun faults (Fig. 1), both of which formed along north-dipping suture zones, bound the South Kunlun Block (Huang, 1977; Xu et al., 1992; Yang et al., 1996; Guo et al., 1998; Yin and Harrison, 2000; Bian et al., 2004; Fig. 1). The Animaqing suture is

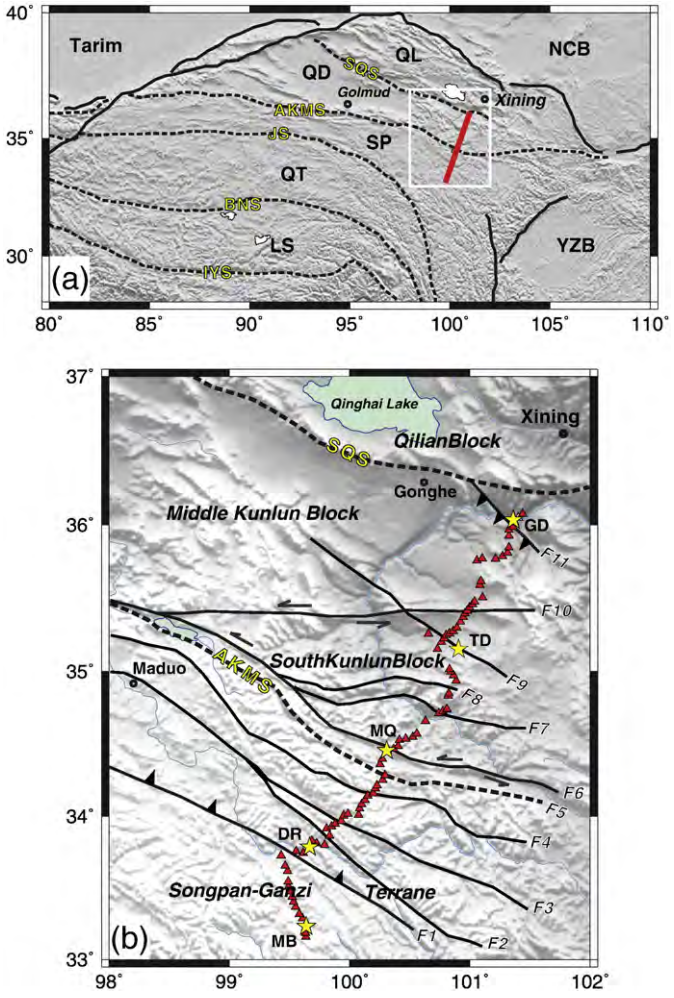

Fig. 1. Upper panel: The topography, terranes or blocks and sutures of the study area. The red line denotes the wide-angle seismic profile. The sutures are denoted by BNS: Banggong-Nujiang suture, JS: Jinsha suture, AKMS: Animaqing-Kunlun-Muztagh suture, SQS: South Qilian suture. The terranes or blocks are denoted by QT: Qiangtang; SP: Songpan-Ganzi; QD: Qaidam; QL: Qilian; NCB: North China Block; YZB: Yangtze Block. Lower panel: Topographic map of the study area. Yellow stars represent positions of the seismic sources (MB: Moba; DR: Dari, MQ: Maqin, TD: Tongde, and GD: Guide), and red triangles represent receivers. Major faults are F1: Fannian-Jilaqu thrust fault; F2: Waershuan-Manrigema; F3: Maduo-Xige in the Songpan-Ganzi terrane; F4: Buqinshan-Jianqiansheng; F5: Zhihaidai-Nianmu and F6: Bokareiketage-Animaqing (equivalent to the SKF) in the Animaqing suture zone; and F7: Dabangshan-Ningmute; F8: Xiadawu-Zhongtie; F9: Yangchuergang-Keerergang; F10: Taxiu-Hekatan equivalent to the MKF; F11: Guomayin-Zheku in the eastern Kunlun mountains (Huang, 1977).

considered to be a Paleo-tethys oceanic subduction zone that dipped northward in the late Paleozoic (Elena et al., 2003). Other geological mapping and geochemical studies have suggested that the east Kunlun southern marginal ophiolite belt represents a Permian–Triassic ocean (Xu et al., 1992; Yang et al., 1996; Wang et al., 1997; Zhu and Helmberger, 1998; Jiang et al., 2000), or a Carboniferous Paleotethyan Ocean (Bian et al., 2004). Our wide-angle seismic profile crosses the major NE faults, including the AKMS zone (F5–F6) and the Middle Kunlun fault (F10) (Fig. 1; Huang, 1977) and provides a new opportunity to examine the crustal structure of these tectonic units.

3. Wide-angle seismic data along the Moba-Guide profile

3.1. Seismic data acquisition and processing

Wide-angle reflection-refraction profiling was carried out by the Institute of Geology and Geophysics, CAS, over a four-month period in 2003. The 380 km-long profile runs from Moba to Guide (Fig. 1).

During the experiment, shots were fired at five sites, from south to north Moba (MB), Dari (DR), Maqin (MQ), Tongde (TD) and Guide (GD) (Fig. 2). In all five locations, the shots consisted of a pattern of holes drilled to a depth greater than 20 m that were then loaded with 3000 to 3500 kg of explosive charges. A total of 100 portable three-component digital DZSS-1 seismographs were installed along the

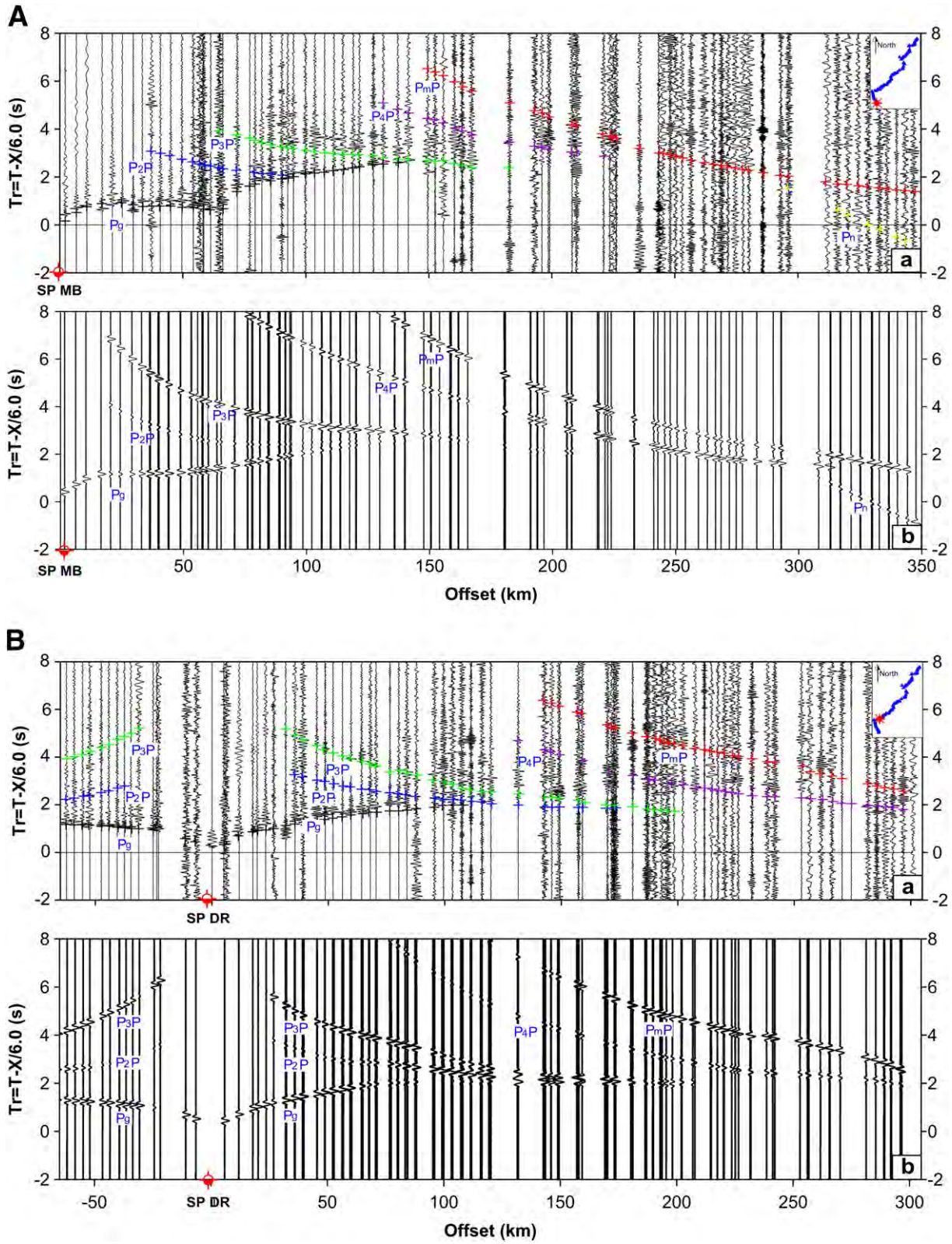

Fig. 2. Reduced P-wave seismic sections for the shots at (A) Moba; (B) Dari; (C) Maqin; (D) Tongde and (E) Guide. Upper panels show the observed data, lower panels show the vertical component of the synthetic data. The reduction velocity is 6.00 km/s. In the upper panels, the seismic data is filtered using a 1–10 Hz bandpass filter. The plus marks show the seismic traveltimes for seismic events in the crust for obtaining the final crustal velocity model as shown in Fig. 4.

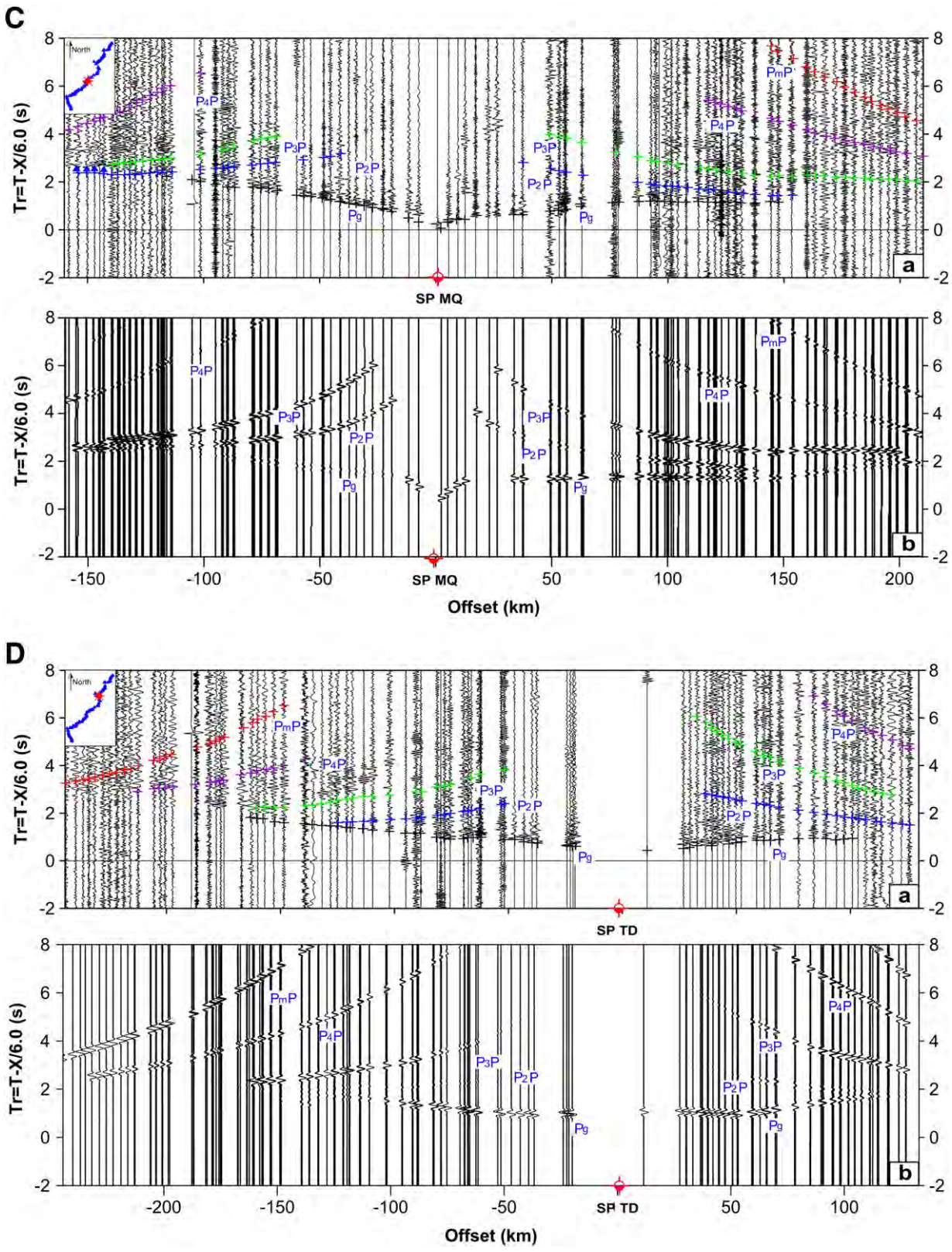

Fig. 2 (*continued*).

survey profile. The average spacing of the stations was 3–4 km and the offset range was 3 to 390 km. The seismic signals recorded by the seismographs were initially sampled at 200 Hz, and then filtered within the 1–10 Hz frequency band for P-waves. The reduction velocity for all shot gathers was 6.0 km/s.

3.2. Description of seismic data

Fig. 2 shows the interpreted *P*-wave record sections. Despite difficult field conditions, almost all the seismograms show a relatively high signal-to-noise ratio. From these record sections we were able to

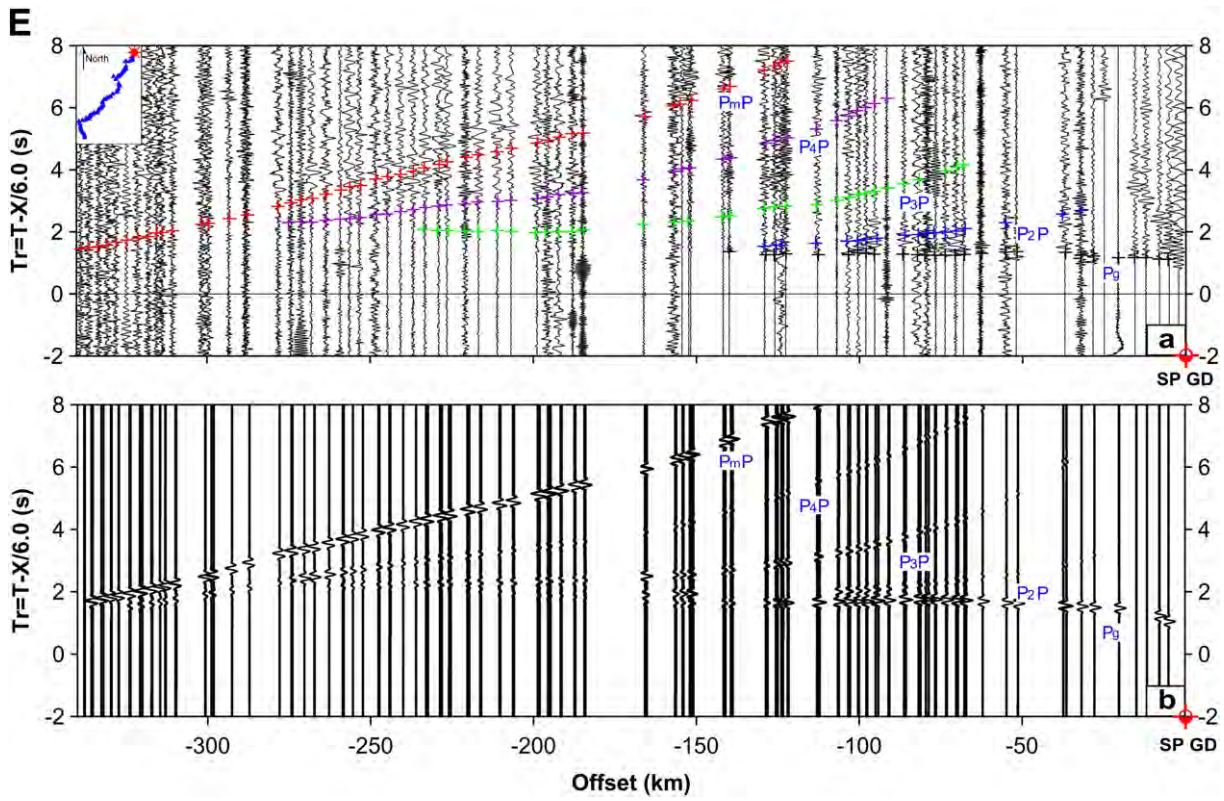

Fig. 2 (*continued*).

identify clearly *Pg* arrivals refracted above the crystalline basement and *PmP*-waves reflected from the Moho. Other seismic events *P2P*, *P3P*, and *P4P*, reflected from the intra-crustal discontinuities (Fig. 3), were identified even though their amplitudes were low compared with the amplitude of the Moho reflection phases.

The event *Pg* can clearly be traced up to the offset 100 km on all shot gathers, and even as far as 160 km (Maqin to the north, Tongde to the south). The variation in the travel times of *Pg* between shotpoints is indicative of considerable lateral heterogeneity above the crystalline basement. For the MB shot (Fig. 2A), the average apparent velocity of the Pg waves is low between the shot and an offset of 20 km, is then constant (about 6 km/s, i.e. horizontal on these displays that use a reduction velocity of 6 km/s) to an offset of 60 km, and then (with delayed travel time of about 0.5 s) abruptly reduces again to the

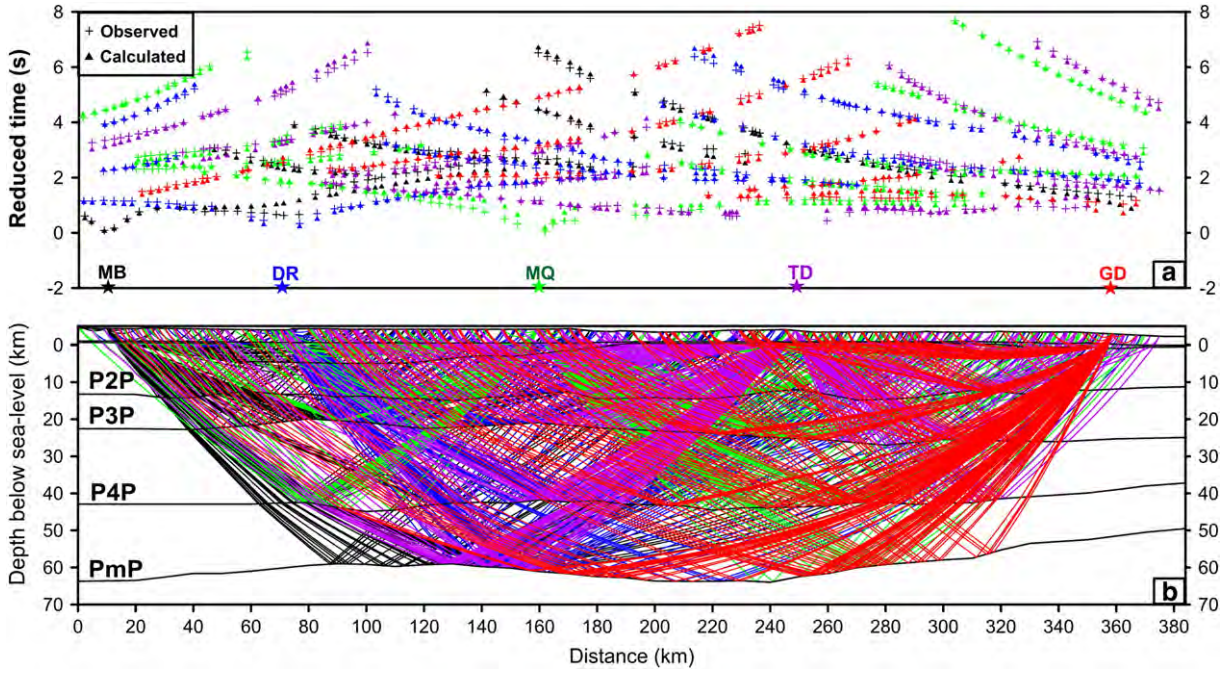

Fig. 3. (a) Comparison between observed (cross) and calculated (triangle) travel times for all crustal reflection events obtained from the five shot gathers; there is consistently good matching between the observed and calculated travel times for all events. (b) Summary diagram showing the seismic ray coverage of the whole crust along the profile.

maximum offset of 140 km. The average apparent velocity of Pg to the southwest of Dari (Fig. 2B) is higher than it is to the northeast. These observations lead to the shallow seismic velocities shown in our final model (Fig. 4) that are slower to the north of Dari than to the south. From MQ (Fig. 2C), the *Pg* travel times to the southwest are considerably delayed in relation to those to the northeast. For the TD shot (Fig. 2D), the *Pg* travel times are almost equal for a given offset compared with those of the opposite observed branches of the shot, which suggests that the lateral heterogeneity of the structure above the crystalline basement is limited in the vicinity of Tongde. For the GD shot (Fig. 2E), *Pg* has a uniform apparent velocity of about 6 km/s, but is delayed by 1 s for arrivals beyond an offset of about 10 km, which implies a lower-velocity basin above the 6 km/s basement.

Three intra crustal *P*-wave reflections (*P2P, P3P, P4P*) were identified from the data obtained. In general, the seismic reflections that corresponded to events *P2P* and *P3P* were well developed. The *P2P* reflections have relatively strong amplitudes compared with those of event *P3P*. The phase of *P2P* could be observed for source-receiver offsets of about 80–220 km for the MB shot (Fig. 2A); 60–140 km for the DR shot (Fig. 2B); 80–160 km in the southwest branch and 80–200 km in the northeast branch for the MQ shot (Fig. 2C); 60–240 km in the southwest branch of the TD shot (Fig. 2D); and 80–220 km for the GD shot (Fig. 2E). *P4P* could be recognized as the first arrival for offsets greater than 160 km on the seismic section of the MB shot (Fig. 2A), and even for offsets greater than 200 km for the DR shot gather (Fig. 2B).

The reflection from the Moho, event *PmP,* could be traced from 160 km to 320 km. Its apparent *P*-wave velocity is in the range 6.6–6.8 km/s. In our final crustal P-wave velocity model, we predicted the event *Pn* of the mantle refraction to be the first arrival at offsets beyond about 280 km (see prediction for the MB shot, Fig. 2A), but this could not be seen in any of our record sections, which is a similar finding to that of other seismic experiments performed in Tibet (e.g. Hirn et al., 1984; Makovsky et al., 1996, 1999; Zhao et al., 2001; Zhang and Klemperer, 2005, 2010; Liu et al., 2006).

4. Wide-angle seismic data interpretation and its uncertainty assessment

4.1. Wide-angle seismic data interpretation

In order to model the seismic events described above, we began by constructing 1-D velocity-depth models using the travel times for each shot. These 1-D models were then combined to provide a starting model for the calculation of a 2-D velocity model. The 2-D model was constructed using a combination of trial-and-error forward modeling of travel times and amplitudes, and inverse modeling of travel times for the shallow structure. For the travel time modeling, the forward problem was solved using classical ray-tracing techniques (Cerveny and Psencik, 1984) for the reflected phases, and an eikonal equation finite-difference solver (Vidale, 1990; Podvin and Lecomte, 1991; Schneider et al., 1992) for the first arrival of the refracted phases. The partial derivatives of the calculated travel times with respect to the velocity and interface nodes were then derived using the techniques described by Lutter and Nowack (1990), Lutter et al. (1990) and Zelt and Smith (1992). A damped least-squares inversion (e.g. Zelt and Smith, 1992) was then applied in order to obtain updates for the velocity and interface nodes, and the forward and inverse problems were then repeated until an acceptable convergence between the observed and calculated travel times had been obtained, yielding the final velocity model of Fig. 4.

The travel time modeling was carried out using a top-to-bottom approach from the upper to the middle and lower crust. In all, 202 *Pg*, 142 *P2P*, 199 *P3P*, 152 *P4P,* and 160 *PmP* readings of travel time were used in the inversion. After eight or nine iterations, the residual travel time for each phase was 0.02 s for *Pg*, 0.14 s for *P2P*, 0.20 s for *P3P*, 0.13 s for *P4P,* and 0.22 s for *PmP*. In order to supplement and guide the travel time modeling, the amplitudes were calculated using dynamic ray tracing (Cerveny and Psencik, 1984). The predicted strong *PmP* reflection amplitudes could barely be observed in our recordings, which could imply a high attenuation of the lower crust throughout the profile.

4.2. Assessment of the uncertainty of the interpretation of the crustal velocity model

Seismic velocity determinations generally yield lower errors than depth determinations. Generally, seismic velocities are accurate to within 3% or ±0.2 km/s, and boundary depths, including the Moho are accurate to within 10% of the stated depth (e.g. Mooney and Braile, 1989). The accuracy of the final crustal velocity model depends on the correct identification of the various phases, the density of the rays, the shot-point interval, and the receiver density (Mooney and Braile, 1989). There are several means of assessing the validation of a final crustal velocity model, for example, by viewing the results of

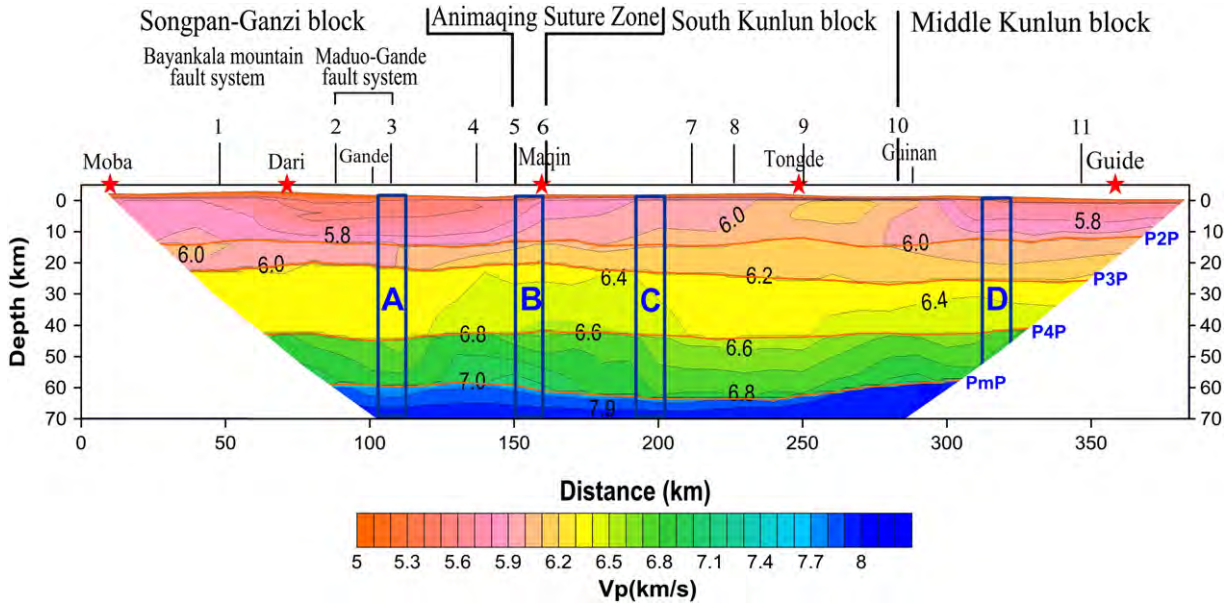

Fig. 4. Crustal velocity model along the Moba-Guide profile, vertically exaggerated by ~50%. The colored region is constrained by ray coverage.

(1) crustal illumination by ray penetration in a specific experiment; (2) the match between the predicted and the observed events; or (3) a checker-board test to estimate the spatial resolution of the model. We herein assess the uncertainty of our final crustal velocity model using ray coverage, the agreement between the predicted and the selected travel times, a checker-board test, and a sensitivity analysis of the P-wave velocity of each node in the crust to the objective function of inversion. Fig. 3b shows the ray coverage of the whole crust by the reflection phases, indicating that the majority of the crust is illuminated rather well by this wide-angle seismic experiment. The validity of our final crustal velocity model was also demonstrated by the satisfactory match between the travel times of the predicted P waves (the dashed lines in Fig. 2A–E) and the visible phases. Worth to mention that, the predicted strong PmP reflection amplitudes are barely observed in the recordings (lower panels of Fig. 2A–F), and could imply a high attenuation of the viscous lower crust (with partial melting, fluids) throughout the profile, or short wavelength heterogeneities, anisotropy and vertical or subvertical structures which leads Moho discontinuity to act as a not strong (but weak) seismic wave velocity gradient belt.

It is noteworthy that for many of the late-arriving phases, a higher degree of uncertainty exists in selecting the arrival times (as much as 0.5 s), which approximately corresponds to the uncertainties in the crustal structure that are of the order of about 3 km ($\approx \pm 0.5s \times 6.2\text{km/}s \approx \pm 3\text{km}$), or the equivalent variations in velocity that are of the order of about 0.08 km/s. In addition, we used a checker-board test to estimate the spatial resolution (e.g. Zelt, 1999). Fig. 4 shows our final interpretation of the whole crustal P-wave velocity model. In order to get a sense of the lateral resolution of the preferred model, we firstly added alternating velocity perturbations of ±0.3 km/s to each velocity node and depth perturbations of ±1.0 km to each depth node of our initial crustal velocity model in the real data traveltime inversion of the wide-angle seismic profile. We then computed synthetic traveltime data from the perturbed model, and inverted these synthetic data to obtain a velocity perturbation pattern (Fig. 5b). We successfully recover the checker-board pattern throughout the illuminated area of the crust, though the amplitudes of the perturbation are typically somewhat reduced. We infer a lateral resolution of about 10 km within the central part of the profile. In order to make a further evaluation of our final crustal velocity model, we estimated the sensitivity of the objective function (Zelt and Smith, 1992) to a change of velocity at each node of the crust. In principle, the more sensitive (or larger) the objective function to the velocity perturbation at one specific node, the more reliable the velocity prediction at that node. Fig. 5c shows the variation of the objective function in the travel time inversion (Zelt and Smith, 1992) to a variation in P-wave velocity of 0.3 km/s at each node in our final crustal velocity model. As expected, shallow structure is better resolved than deeper structure, though acceptable velocities are expected throughout the crust (Fig. 5c).

5. Crustal velocity model along the Moba-Guide profile

5.1. Sedimentary cover (surface to 5.9 km/s)

The shallow velocity structure reveals the geometry of the sedimentary basins along our profile. Strong lateral variations in basin thickness and composition may be inferred from the variations in P-wave velocity in the range 3.8–5.9 km/s. We infer that the poorly resolved velocities of <4.5 km/s, which are at most 1 km thick in our profile, represent Cenozoic fill of the intramontane Gonghe-Guide basin (e.g. Fang et al., 2005) at the extreme north end of the profile, and scattered Neogene/Quaternary deposits elsewhere. The most widespread (meta-) sedimentary outcrops along the profile are the Middle to Late Triassic Songpan–Ganzi complex, which consist of deformed, greenschist-grade turbidites, with an estimated stratigraphic thickness of 10 km, reaching 15 km locally (Weislogel, 2008). Laboratory measurements suggest that metagreywackes of zeolite- to greenschist grade are characterized by seismic velocities of 5.5 ± 0.6 km/s in the upper 10 km for typical geotherms (Christensen and Mooney, 1995). In contrast, granitic gneiss has a seismic velocity of 6.1 ± 0.1 km/s in the same depth and temperature range. We therefore used our 5.9 km/s iso-velocity contour as a proxy for the base of the Songpan–Ganzi flysch throughout our profile, and inferred the presence of two major sedimentary basins. The maximum thickness of the sedimentary rocks appears to be up to 15 km from the South Kunlun fault southwards as far as Dari (at distances km 150 to km 50 along the profile, Fig. 4), and probably continues at this thickness as far as the south end of the profile assuming that the metamorphic grade or the proportion of slate, both of which are associated with higher seismic velocities, increases to the south of the Fannian–Jilaqu thrust fault (F1 in Fig. 1b). Around Tongde, where the seismic velocity reaches 6.0 km/s within 2 km of the surface, any Songpan–Ganzi flysch is probably very thin, though we cannot exclude the possibility that the flysch remains >10 km thick, but here entirely dominated by calcareous lithologies. Limestones of low porosity are typically characterized by velocities of about 6 km/s (Wyllie et al., 1956), reaching 6.8 km/s for marbles (Christensen and Mooney, 1995). If the outcropping 'marine limestone or sandstone' (Pan et al., 2004) were found to continue to the depth of 15 km, it would be possible to use a suitable variation of the ratio of calcareous to siliceous rocks to match the observed velocities (5.9–6.1 km/s), even for a total basin thickness of 15 km, as observed elsewhere along the profile. Everywhere between the South and North Kunlun faults the inferred sedimentary thickness depends critically on assumptions about local lithologies, but is likely far thinner than either to the south or to the north. The second clear major accumulation of sedimentary rocks, which is up to 10 km thick, is present in the Middle Kunlun block, from the MKF (here known as the Taxiu–Hekatan fault (F10 in Fig. 1b), to the north end of the profile beneath the much younger Guide basin.

This lateral variation of sedimentary thickness along the profile is consistent with the differences in delays in *Pg* travel time and in the apparent velocities obtained from the shot gathers (Fig. 2) described in Section 4.2. The maximum visible offset of the *Pg* phase (as far as 160 km) is much larger than is typically observed in other parts of Tibet, including the Himalayan, Lhasa, and Qiangtang terranes (see e.g. Hirn et al., 1984; Teng et al., 1985; Makovsky et al., 1996, 1999; Zhao et al., 2001; Zhang and Klemperer, 2005, 2010; Liu et al., 2006). The greater distance over which this seismic phase may be observed is probably due to the absence of low velocities in the near-surface data (no Tertiary basins except beneath the northern shotpoint at Guide on the edge of the Gonghe Basin), the rather low vertical velocity gradients through the Songpan–Ganzi flysch, and the gradual velocity increase in the upper-crustal basement to a depth of 20–25 km.

5.2. Upper crustal basement (5.9 km/s to P3P)

The layer that has a *P*-wave velocity ≥ 5.9 km/s may be interpreted as being the Yangtze (South China) basement, in the southern part of the profile. The base of the Songpan–Ganzi flysch may correspond locally to the wide-angle reflection *P2P*, and might represent the inferred large-scale decollement between the Triassic flysch and the Yangtze block (Xu et al., 1992; Mattauer et al., 1992; Calassou, 1994). Further north along our profile, this wide-angle reflection is of unknown origin within the granitic basement.

It is sometimes assumed that the Songpan–Ganzi and the Kunlun blocks have the same Yangtze crystalline basement (Yang et al., 1986; Rao et al., 1987; Xu et al., 1992). Although there are large differences in the thicknesses of the upper crustal rocks (velocities 5.9–6.2 km/s, extending down to *P3P*) i.e. 8–10 km thickness in the Songpan–Ganzi terrane, and in the Middle Kunlun block, but up to 25 km in the South

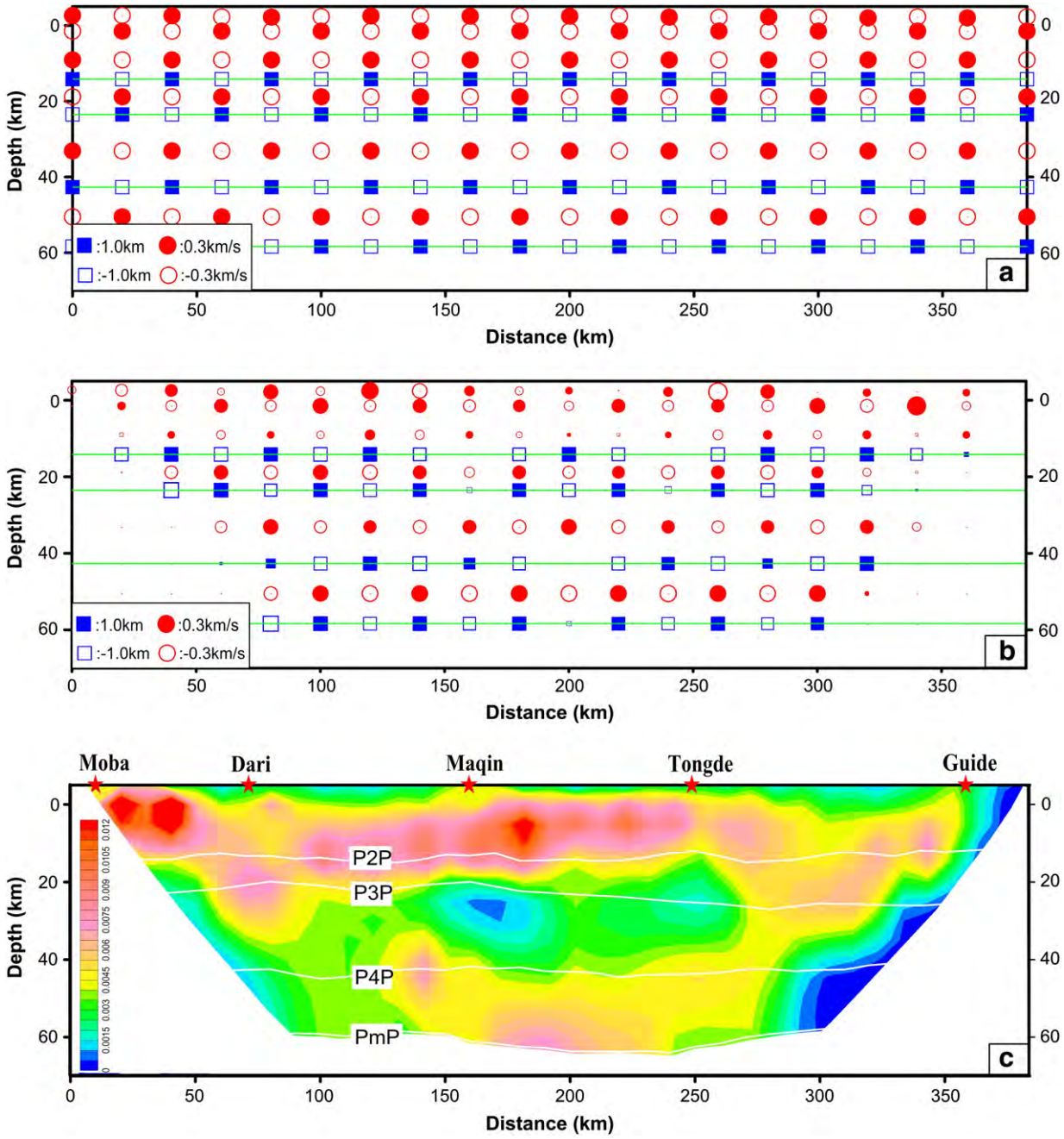

Fig. 5. Checker-board tests of the final crustal P-wave velocity model of Fig. 4. (a) Perturbations of ± 0.3 km/s at each velocity node and ± 1.0 km at each reflector node applied to initial crustal velocity model in the traveltime inversion along the wide-angle seismic profile, and used to calculate synthetic travel time data for inversion; (b) Results of inversion of synthetic data show that around the center part of the profile the HVA and LVA are alternately distributed and resemble the checker-board model in Fig. 5a. This could provide a validation of our final crustal velocity model within the center part area of the profile; (c) Objective function variation in the travel-time inversion (Zelt and Smith, 1992) to a velocity perturbation of 0.3 km/s at each node in our final crustal velocity model.

Kunlun block, it is unclear whether or not this marks a major change in the crystalline basement between these blocks. It is possible that the South Kunlun block is simply a basement high that did not receive as much Triassic sedimentation as adjacent blocks, or that this is a region of more intense granite formation that occurred during the widespread crustal melting and granite intrusion episodes that immediately followed the terminal deposition of the Songpan–Ganzi flysch and the final accretion of the Songpan–Ganzi block to north China (e.g. Roger et al., 2004). Nonetheless, the large changes in velocity across the Animaqing suture zone in the middle and lower crust argue that there is a fundamental change in basement type between the Songpan–Ganzi terrane and the Kunlun blocks.

5.3. Middle crust, Lower crust and Moho (P3P to PmP)

The middle crust, which is constrained by modeling reflections *P3P* and *P4P* from top and bottom, shows modest changes in thickness along the profile. The thickness of the middle crust is about 22 km under the Songpan–Ganzi terrane. Then, it gradually thins to about 16 km at the north end of the profile. The velocity that characterizes the middle crust also changes slightly but systematically, from 6.35 km/s beneath the Songpan–Ganzi terrane to 6.45 km/s beneath and immediately north of the surface trace of the AMKS zone, then decreases again to 6.35 – 6.4 km/s further to the north in the South and Middle Kunlun blocks.

The lower crust (*P4P* to *PmP*) also varies in thickness, increasing gradually from 16 km in the Songpan–Ganzi terrane to 20 km in the AMKS zone and South Kunlun block, then to 16 km in the Middle Kunlun block (Fig. 4). Lower-crustal P-wave velocities are 6.6–6.9 km/s beneath the Songpan-Ganzi terrane, 6.6–7.1 km/s under the southern East-Kunlun block, and 6.5–6.8 km/s under the middle East-Kunlun block. The lower-crustal velocities are correlated positively with those of the middle crust. Thus, lower lower-crustal velocities are seen in the Songpan-Ganzi terrane and South Kunlun block which have relatively lower middle-crustal velocities of 6.0–6.4 km/s, and higher lower-crustal velocities are seen beneath the AKMS zone and beneath the Middle Kunlun block which have higher mid-crustal velocities of 6.4–6.5 km/s. These higher lower-crustal velocities could be associated with the AKMS, are possibly related to the melting events that produced Jurassic–Cretaceous granites (Pan et al., 2004).

Many tectonic models (e.g. Yin and Harrison, 2000) assume that the Songpan–Ganzi flysch was initially deposited on oceanic crust. Such a crust should be characterized by velocities exceeding 7 km/s over a thickness of at least 5 km, when buried to any significant depth (e.g. Shillington et al., 2009). Velocities consistently above 7 km/s are present nowhere along our profile, nor indeed in any of the profiles compared in Fig. 6 (Zhang, 2001).

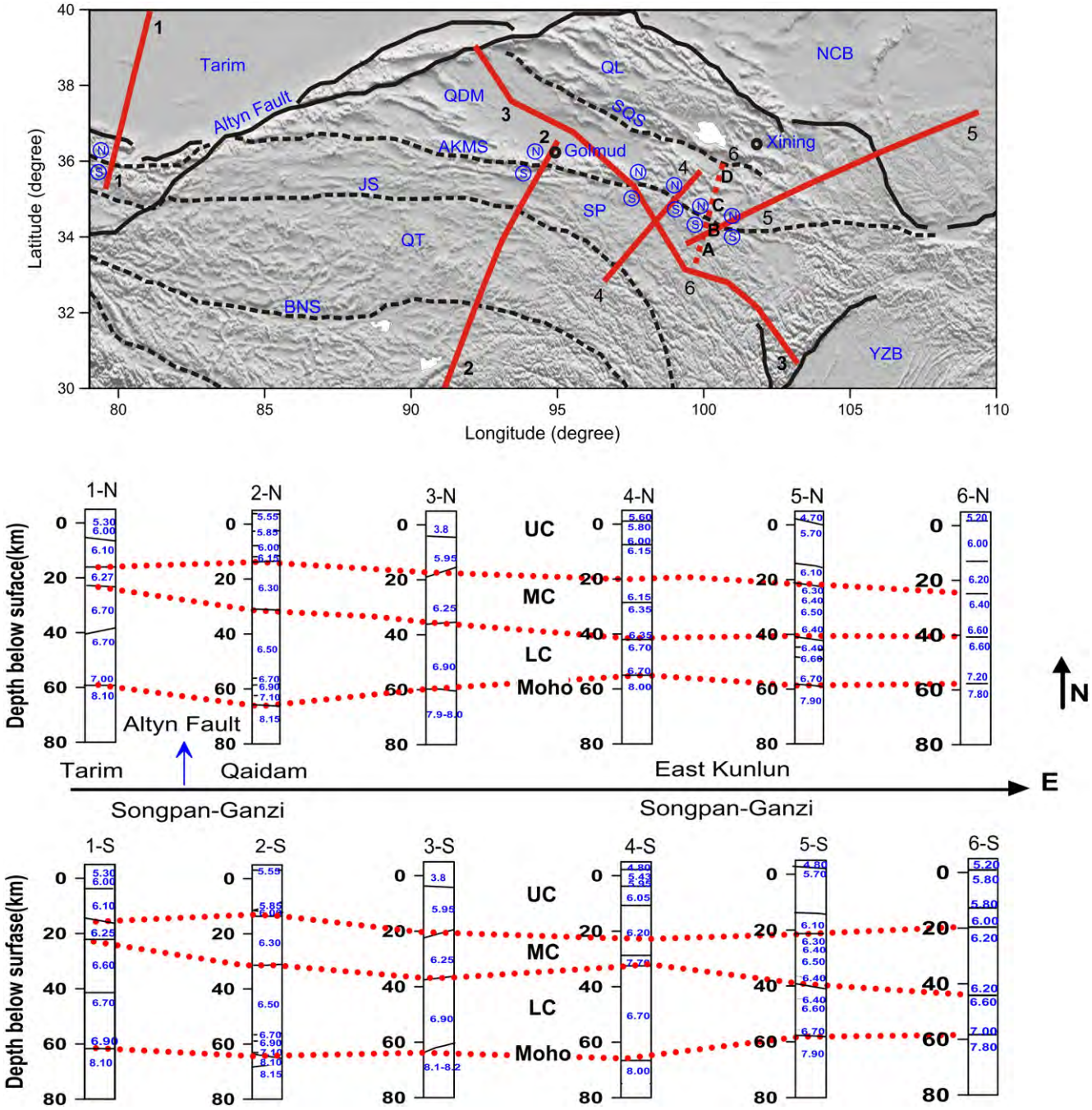

Fig. 6. Comparison between our crustal model along the Moba-Guide profile with other regional teleseismic and active source seismic profiles. N and S refer to north and south of the AMQ suture, or of the Kunlun fault. Profile 1: Tarim basin West Kunlun profile (Li et al., 2001); Profile 2: Qaidamu basin-Yadong active source seismic transect (Wu et al., 1993) and Gulu-Golmud passive source seismic profile (Vergne et al., 2002); Profile 3: Sichuan basin-Tarim basin wide-angle seismic profile (Wang et al., in press); Profile 4: Yushu-Gonghe active source profile (Galvé et al., 2002) and passive source seismic profile (Vergne et al., 2002); Profile 5: 1000 km-long Darlag–Lanzhou–Jingbian seismic refraction profile (Liu et al., 2006) and Profile 6: Moba-Guide active source seismic profile (this study). Bottom: 1D velocity-depth functions from each profile.

Crustal thickness varies only slightly along the profile, masking more important variations of layer thicknesses along the profile. The Moho deepens slightly in the central portion of the profile, from about 62 km under the Songpan–Gangzi terrane to 65 km immediately north of the AMKS, and then shallows to about 60 km under the Kunlun blocks at the north end of the profile. (These are depths below sea-level; add c. 2 km for the true crustal thickness.) Although likely uncertainties in Moho depth are of the same order as the inferred lateral variation in crustal thickness along the profile, we note that the highest lower-crustal velocities reach 7 km/s and occur immediately above the shallowest inferred Moho, to the south of Maqin and to the north of Tongde, and that the lowest lower-crustal velocities ($\leq$6.8 km/s) occur above the deepest Moho between Maqin and Tongde. Relatively higher velocities (>6.8 km/s) beneath Kunlun fault may be seismic evidence of crust contamination with mantle material. If the lower-crustal velocity were laterally more uniform, this would accentuate the proposed Moho topography. Hence we suspect that the Moho deepening between Maqin and Tongde is a real characteristic of the lithosphere here. The relatively large shot spacing (~100 km) results in poor lateral resolution of any potentially sharp structures; hence we are not able to distinguish between gradual crustal thickening and possible abrupt Moho offsets that occur across the Kunlun or other faults.

5.4. Crustal properties of tectonic units along the Moba–Guide profile

The seismic velocities reveal differences in crustal structure and composition between the Songpan–Ganzi terrane, the South Kunlun block and the North Kunlun block (Fig. 4). The combined thickness of the middle and lower crust varies by about 20%, from about 38 km under the Songpan–Ganzi and the southern East Kunlun blocks to 32 km under the middle East Kunlun block. The total thickness of the crustal basement (excluding 0–15 km of sedimentary cover) varies from 44 km in the Songpan–Ganzi terrane, to a maximum of 64 km beneath Tongde in the South Kunlun block where there is essentially no sedimentary cover, to 48 km in the middle East Kunlun block. This variability suggests that the three blocks may have independent origins and deformation histories. Between these blocks, the AKMS may be identified with about 0.2 km/s higher P-wave velocities in the middle and lower crust, in addition to lateral P-wave velocity variation of upper crust beneath the segment bounded by Fault 5 and Fault 6.

The tectonic blocks in the studied area experienced long-term tectonic events, and their crustal structures display complicate imprints upon at least Paleozoic collision and Cenozoic deformation from the collision between Indian and Eurasia plates. Before the determination of particular crustal property, we make the comparisons between the global average crustal velocity-depth curve by compiling interpretational results of wide-angle seismic profiles of the World (Christensen and Mooney, 1995) and tectonic blocks in this study in this discussion and make the similar discussion of depth-curves between particular tectonic block with continental arc in the discussions next. In order to compare the tectonic units crossed by our profile, we selected the locations of columns A–D (Fig. 4) where the ray coverage, and therefore the velocity resolution, were sufficient to provide good characterization of Songpan–Ganzi, the AKMS fault belt, the southern and the middle East Kunlun blocks (Fig. 3), and for comparison to the velocity-depth curves of an average continental crust (Christensen and Mooney, 1995) (Fig. 7a). Fig. 7b makes a similar comparison of velocities averaged along strike of each crustal block, using other controlled-source seismic profiles (Darlag–Lanzhou–Jingbian (Liu et al., 2006), Sichuan basin-Tarim basin (Wang et al., in press) and Moba–Guide (this study) (Fig. 7), and confirms that the conclusions we draw below can be generalised along-strike rather than being very local properties along our profile.

5.4.1. Different thickness of Triassic flysch

From our final crustal P-wave velocity model, we infer the thickness of the Songpan–Ganzi flysch is about 15 km to the south of the Animaqing suture zone, which is similar to the estimated stratigraphic thickness of 10 or locally 15 km (Weislogel, 2008). It has a thickness of about 10 km in the Middle Kunlun block, with thicknesses in the AKMS and South Kunlun block that depend on assumptions about the lithologies.

The relatively abrupt and significant changes in thickness of the Songpan–Ganzi flysch across both the South Kunlun and the Middle

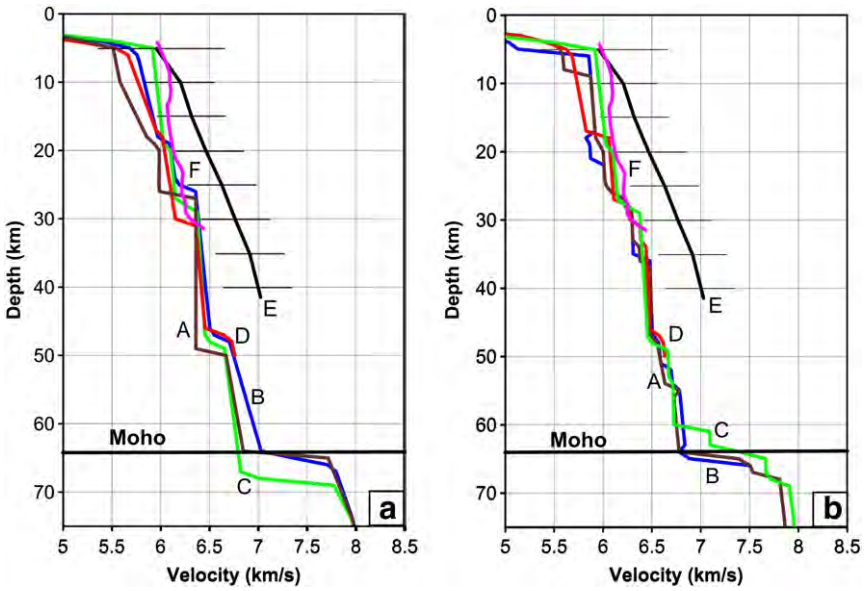

Fig. 7. (a)Velocity-depth functions along the Moba-Guide active source seismic profile (this study) (lines A, B, C and D correspond to columns A, B, C and D in Fig. 4 in Songpan-Ganzi terrane, the AKMS zone, and the South and Middle Kunlun blocks, respectively) compared to the global average velocity-depth curve for continental crust (Christensen and Mooney, 1995; line E) and the southern Sierra Nevada continental arc (Fliedner et al., 2000; Line F); (b) As (a) but now averaging velocity-depth profiles along-strike of the AKMS and South and Middle Kunlun blocks (for data sources see Fig. 6) (Liu et al., 2006; Wang et al., in press; and this study). Where, velocity-depth curves of the upper mantle (beneath Moho) come from Pn travel time tomography (Liang and Song, 2006).

Kunlun faults (F6 and F10 in Fig. 4), could suggest that these faults mark the juxtaposition of separate blocks with separate accumulations of Songpan–Ganzi flysch. One possible alternative explanation that uplift of the South Kunlun block led to accelerated erosion between the SKF and the MKF, is not favored because there is no evidence for the uplift of the deeper iso-velocity contours. The limited lateral resolution of our wide-angle seismic profile means that we cannot distinguish abrupt thickness changes across a fault from any gradual changes that might be due to facies transitions; hence, it is not clear whether the southward increase in velocity around Dari could be directly related to the Fannian–Jilaqu thrust fault (F1).

The northward thinning of the Triassic flysch from the Songpan–Ganzi terrane to the South Kunlun block suggests that these sediments may be derived mainly from the Songpan–Ganzi terrane itself or from the Yangtze block and/or from denudation of exhumed metamorphic rocks from the eastern China block (Nie et al., 1994), and not derived mainly from the southern margin of the North China block (Avigad, 1995; Bruguier et al., 1997). Similarly, the southward thinning of the Triassic flysch from the Middle to the South Kunlun block suggests that these sediments may be derived mainly from the north or east, and raises the possibility of two independent sources for the deepest accumulations we infer, in the Songpan–Ganzi terrane and in the Middle Kunlun block.

5.4.2. Intermediate-felsic crust

In the Songpan–Ganzi terrane and Middle Kunlun blocks, and in the South Kunlun block below 15 km, the P-wave velocity gradient (new curve and existing curves A, C and D, Fig. 7) agrees well with that of the average continental crust (Christensen and Mooney, 1995), but the absolute velocity is lower by 0.5 km/s than the continental average. Even allowing for the burial of the Songpan–Ganzi terrane and Middle Kunlun block by c. 10 km of Triassic flysch, and moving these curves up by 10 km, the deviation from typical crust is still c. 0.25 km/s. These crustal velocity values suggest the crusts of the Songpan–Ganzi and the Middle Kunlun blocks are more felsic than normal. Another possibility is that crustal temperatures beneath our profile are 500 °C above typical continental geotherms (Christensen, 1979). If it is the case, then crustal Vp/Vs ratios should be much higher than 1.73 as Vs values will remarkably decreased (Zhang et al., 2009, 2010b), which is not consistent with average crustal Vp/Vs ratios obtained from the Yushu–Gonghe passive-source seismic experiment (Vergne et al., 2002) of 1.74–1.75 under the Songpan–Ganzi block, and 1.73 under the Middle Kunlun block. So, we don't prefer to the alternative interpretation that crustal temperatures beneath the profile are 500 °C above typical continental geotherms.

5.4.3. Southern East-Kunlun block: a continental arc?

In contrast to the Songpan–Ganzi and Middle Kunlun terranes that have velocity-depth functions that, after allowance for the Triassic flysch, are only slightly below the continental average, the South Kunlun block, that appears to have only a thin Triassic flysch sequence, must be significantly more felsic. Our final model (Fig. 4a) shows P-wave velocities of 5.9–6.1 km/s in the upper crust with only a very slight vertical velocity gradient. This low velocity gradient is one characteristic of continental arcs, as studied for example in the active Alaskan Peninsula (Fliedner and Klemperer, 2000) and the Mesozoic Sierra Nevada, California (Fliedner et al., 2000; Lerch et al., 2007; Takahashi et al., 2008), the latter also showing strikingly low velocities. Curve B from Fig. 7 a and b superimposed on the velocity-depth function of the southern Sierra Nevada continental arc (Fliedner et al., 2000). The similarity encourages us to suggest that the crust beneath the southern Kunlun block formed as a continental arc. We hypothesise that the AKMS represents the Paleozoic collision between continental crust of the Songpan–Ganzi terrane and a continental arc of the South Kunlun block, which can be further supported by tectonic studies in western Kunlun orogenic belt (Xiao et al., 2001, 2002; Wang et al., 2001a,b; Ye et al., 2008).

6. West-east variation of crustal structure along the Kunlun fault

The structure of the crust and upper mantle in different segments of the Kunlun belt have been studied since the 1990 s by a range of seismic experiments (Fig. 6). Teleseismic studies have included the Gulu–Gelmu and the Yushu–Gonghe profiles (Vergne et al., 2002, profiles #2 and #4, and Zhu and Helmberger, 1998 #2, in Fig. 6). Active source seismic profiles have included the Qaidam basin-Yadong transect and INDEPTH-4 profile (Wu et al., 1993; Karplus et al., in prep; Zhao et al., 2008; #2 in Fig. 6); the Shichuan basin-Tarim basin wide-angle seismic profile (Wang et al., in press; #3 in Fig. 6); the Yushu–Gonghe active source profile (Galvé et al., 2002; Jiang et al., 2006; #4 in Fig. 6); the 1000 km-long Xiachayu–Gonghe wide-angle seismic profile (Zhang et al., 2003); the 1000 km-long Darlag–Lanzhou–Jingbian seismic refraction profile (Liu et al., 2006; #5 in Fig. 6); and our Moba-Guide profile (this study; #6 in Fig. 6). Profiles #2–6 all cross the eastern part of the East Kunlun fault. In addition, the Tarim-west Kunlun profile (active-source: Li et al., 2001, passive-source: Kao et al., 2001; Wittlinger et al., 2004) (#1 in Fig. 6) crosses the west Kunlun fault.

These profiles provide an excellent opportunity to discuss the west-east variation in crustal structure along the Kunlun fault and AKMS by comparing 1-D crustal velocity columns from either side of the fault (Fig. 6b).

The most robust feature of crustal seismic studies is normally the depth to the Moho or crustal thickness. The Kunlun fault system and suture is sometimes regarded as the northern edge of the Tibetan plateau. Fig. 6 suggests that east of 99°E (profiles #5 and #6) crustal thickness is about 62–64 km, and does not change significantly across the AKMS or South Kunlun fault. Further west, profiles #2, 3 and 4 show gradually increasing crustal thickness, as the mean elevation of the Tibetan plateau also rises slightly. In none of these profiles is there evidence for a Moho offset associated with the Kunlun strike-slip fault, though beneath the Gonghe basin (profile #4) and the Qaidam basin (profile #2) crustal thickness is c. 10 km less than beneath the high plateau. Neither the active- nor passive-source data along profile #4 are of sufficient quality to define whether this change in crustal thickness is abrupt or gradational; whereas along profile #2 both the active- and passive-source data constrain the >10 km Moho offset to be at least 50 km north of the Kunlun strike-slip fault (Karplus et al., submitted for publication; Zhu and Helmberger, 1998; Vergne et al., 2002). This offset could possibly be related to the AKMS zone dipping 45° or less through the entire crust. Moho offsets reported from passive seismic data along profile #1 in far western Tibet (Kao et al., 2001; Wittlinger et al., 2004) may likely be related to the Altyn Tagh strike-slip fault, as it is not clear that the Kunlun strike-slip fail exists as a separate entity that far west.

The other significant change from east to west is in the thickness of the lower crust, with velocities exceeding ~6.5 km/s, and the middle crust, velocities ~6.2–6.5 km/s. Our profile #6 at 100°E shows the Songpan–Ganzi terrane has ~20 km thickness of lower crust and ~20 km thickness of middle crust; but profiles #2, #3 and #4 from 93° to 98°E have 30–40 km thick lower crusts, and correspondingly thinner middle crusts. Thus the increased crustal thickness from 93° to 98°E compared to that at 100°E is largely achieved by thickening of the lower crust, perhaps indicating a crustal flow mechanism operating more strongly in the western region. If our hypothesis is correct that the AKMS represents the Paleozoic collision between continental crust of the Songpan–Ganzi terrane and a continental arc of the South Kunlun block. This E–W variation of the crustal thickness can be alternatively well due to differences in the thickness of the crust of the two plates before their collision (with a paleo-Moho possibly at a depth of about 20–30 km where we place the middle crust in our crustal P-wave velocity model).

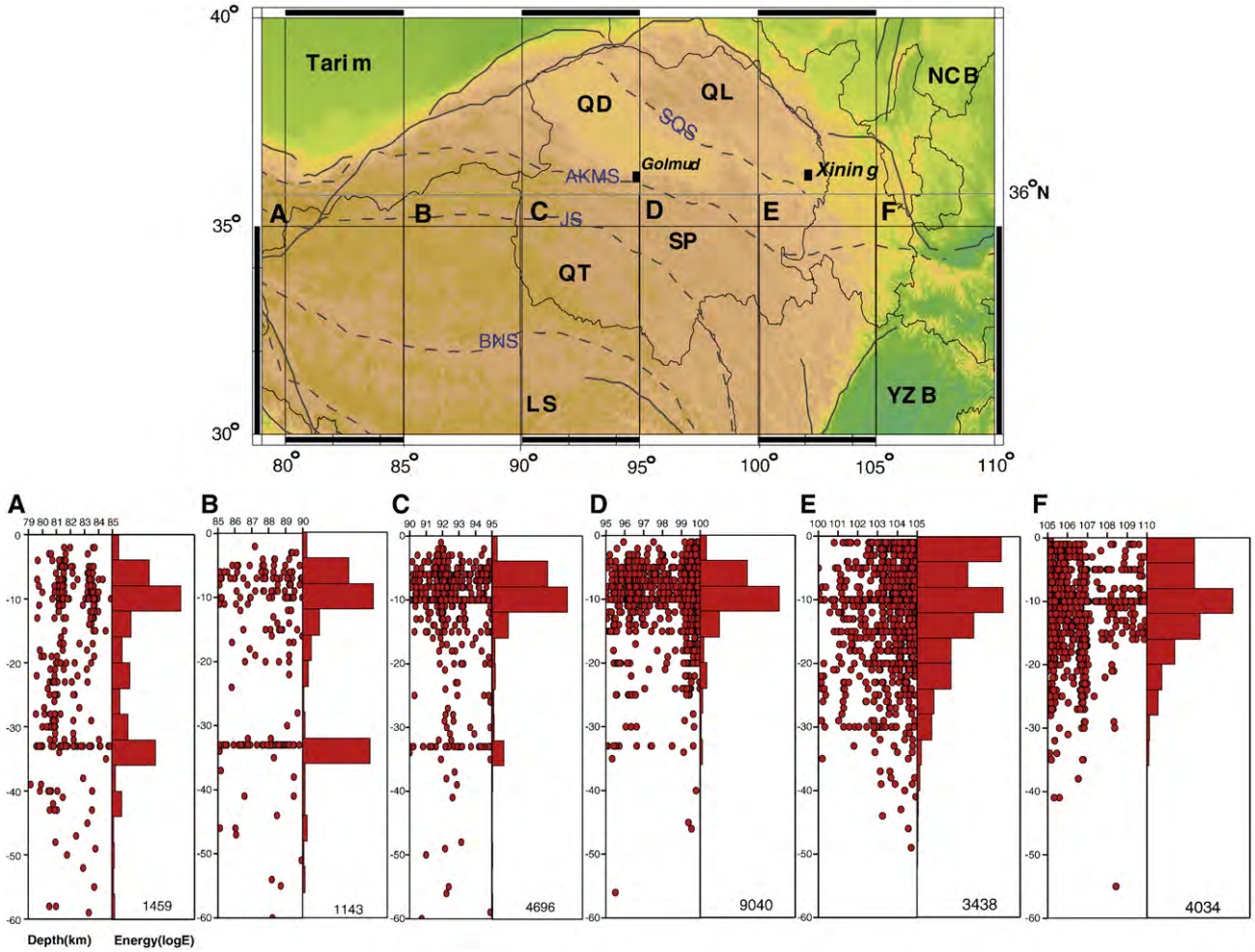

Fig. 8. Upper panel: the locations of six cells A-F at south of 36°N; Lower panel: The hypocentres with depth (upper 60 km of the Earth model) on the leftmost graph and related logE–h distribution of earthquakes on the rightmost graph for each cell. The hypocentres with depth are denoted by red dots. The filled red bars histogram represents the energy of all earthquakes from the catalogue for 1980–June 2010 provided by China Earthquake Network Center. At the bottom of this graph the cell label, the maximum of the energys logarithm logEmax are given. The normalizing value of the maximum of the energy's logarithm logEmax is given on the horizontal axis of the energy-depth distribution graph.

If this is the case there is no need to invoke material flux in the deeper crust. The presence of a material flux in the lower crust would be expected to be recorded in elevated heat flow and the consequently attenuated brittle behavior of the lower crust, i.e. lower level of seismic energy release. In the following, we evaluate the rheology property of lower crust by considering the distribution of hypocenters and of seismic energy released versus depth as a proxy to rheology by taking the similar scheme proposed by Panza and Raykova (2008). We investigated this by studying the structure and rheology of the crust by compiling earthquake events during 1980 and 2010 in available earthquake Catalog from China Earthquake Network Center. As the depths of only a few earthquake events are determined for Songpan-Ganzi and Qaidam–East Kunlun terranes with limitation of non-dense permanent seismic stations in Tibet, we make statistics of seismic events in six cells 5° by 5° in size (upper panel of Fig. 8), which can be used to analyze crustal rheology roughly for our discussion. Where, seismic energy (E) is inverted from earthquake magnitude (Ms): $\log E = 11.8 + 1.5Ms$. We have given a synoptic representation of the mechanical properties of the uppermost 60 km, along with the seismicity. Fig. 8 displays the depth (h)-earthquake distribution (left, lower panel of Fig. 8) and log E–h distribution (right, lower panel of Fig. 8) for 6 cells south of 36°N. We can observe that, even though these six cells include earthquake occurrences in Songpan–Ganzi (SP-GZ), Qiangtang (QT) and northern part of Lhasa terranes, a classic Coulomb/Byerlee (brittle/ductile) transition is still valid in cells D, E and F (from 90° to 100°E) shown as lower panel of Fig. 8, where the rheology and mechanical properties of rocks follow the Sibsons law for the upper crust, and a power law creep in the lower crust (Panza and Raykova, 2008), the earthquake energy is concentrated in the upper crust (<30 km) (Gao et al., 2000). The pattern difference of seismic energy release between two cell groups (one group consisting of cells A, B and C, and another of cells D, E and F) may suggest the west-east difference of leading edge of the subducting Indian crust/lithosphere. From these results in Fig. 8, it is preferred to propose that crustal thickness increases from 93° to 100°E (largely achieved by thickening of the lower crust) probably governed by a lower crustal flow mechanism (Royden et al., 1997; Klemperer, 2006; Zhang et al., 2009) even though we could not neglect the possibility of differences in the thickness of the crust of the two plates before their collision, and/or joint contributions of them.

7. Conclusions

Our interpretation of the Moba–Guide wide-angle seismic profile suggests the following conclusions:

1) Three tectonic belts under the Moba–Guide profile, i.e., the Songpan–Ganzi terrane, the Southern Kunlun block, and the Middle Kunlun block can be distinguished based on their seismic characteristics. Crustal thickness varies from ~62 km under the Songpan–Ganzi terrane, then increases to as much as 64 km under the South

Kunlun block, and decreases to 60 km under the Middle Kunlun block.

2) The Songpan–Ganzi Triassic flysch seems to be present to a depth of 15 km in the Songpan–Ganzi terrane, and to a depth of 10 km in the Middle Kunlun block, with interpreted thickness in the South Kunlun block much less, though dependent on assumptions about lithologies. We suggest that the relatively abrupt and significant changes in thickness along the profile mark the juxtaposition of separate blocks with separate accumulations of Songpan–Ganzi flysch.
3) Our crustal velocity model suggests that the crust of the Songpan–Ganzi terrane and the Middle Kunlun block, beneath the Triassic flysch, is continental, and not oceanic as suggested by some earlier studies (Jiang et al., 2000; Wang et al., 2001a,b; Xiao et al., 2001; Bian et al., 2004).
4) The South Kunlun block is characterized by a low vertical velocity gradient and low velocities (compared to average continental crust, though higher than adjacent flysch accumulations), and is inferred to be a continental arc, juxtaposed against the Songpan–Ganzi terrane by the AKMS. Our highest observed velocities of 6.9–7.0 km/s are located vertically beneath the AKMS, and may be related to trapped fragments of oceanic crust, or to the melting events that produced Jurassic–Cretaceous granites.
5) The analyses of the crustal velocity columns of the related wide-angle seismic profiles across the East Kunlun fault belt indicate a remarkable lateral variation in Moho topography from the west to the east of the fault belt (15–20 km Moho step beneath Qaidam, and 2–5 km under our profile); the lower crustal thickness remains constant (at about 35 km) between longitude 80°E and 95°E, which suggests that similar thrust-thickening processes have played a role where the Qaidam Basin abuts the Kunlun fault. The increased crustal thickness from 93° to 98°E compared to that at 100°E may be due to differences in the thickness of the crust of the two plates before their collision, and/or largely achieved by thickening of the lower crust, perhaps indicating a crustal flow mechanism operating more strongly in the western region.

Acknowledgments

The authors gratefully acknowledge the financial support provided by the Chinese Academy of Sciences (KZCX2-YW-132) and the National Nature Sciences Foundation of China (40721003, 40830315). We would also like to thank staff of the Institute of Geology and Geophysics, the Chinese Academy of Sciences; the Geology Samples Centre and the Second Geophysical Exploration Brigade of the Ministry of Land and Resources of China (MLRC); and the Geological Research Academy, Guangxi Province, for their efforts in the acquisition of seismic field data. We would particularly like to thank J.E. Vidale and C.A. Zelt for providing the inversion software used in this study. Constructive comments made by Professors M. Santosh, D. Panza, W.J. Xiao, T. Pares and other reviewers were most gratefully received.

References

Arnaud, N.O., Vidal, P., Tapponnier, P., Matte, P., Deng, W.M., 1992. The high K2O volcanism of northwestern Tibet: geochemistry and tectonic implications. Earth and Planetary Science Letters 111, 351–367.
Avigad, D., 1995. Exhumation of the Dabie Shan ultra-high-pressure rocks and accumulation of the Songpan-Ganzi flysch sequence, central China. Comment. Geology 23, 764–765.
Bian, Q.T., Li, D.H., Pospelov, I., Yin, L.M., Li, H.S., Zhao, D.S., Chang, C.F., Luo, X.Q., Gao, S.L., Astrakhantsev, O., Chamov, N., 2004. Age, geochemistry and tectonic setting of Buqingshan ophiolites, North Qinghai–Tibet Plateau, China. Journal of Asian Earth Sciences 23 (4), 577–596.
Bruguier, O., Lancelot, J.R., Malavieille, J., 1997. U–Pb dating on single detrital zircon grains from the Triassic Sonpan–Ganze flysch (Central China): provenance and tectonic correlations. Earth and Planetary Science Letters 152, 217–231.
Burchfiel, B., Molnar, P., Zhao, Z., Liang, K., Wang, S., Huang, M., Sutter, J., 1989. Geology of the Ulugh Muztagh area, northern Tibet. Earth and Planetary Science Letters 94, 57–70.
Burchfiel, B.C., Chen, Z., Liu, Y., Royden, L.H., 1995. Tectonics of the Longmenshan and adjacent regions. International Geology Review 37, 661–735.
Calassou, S., 1994. Étude tectonique d'une chaîne de décollement: A) tectonique et Tertiaire de la chaîne de Songpan–Garzê; B) géométrie et cinématique des déformations dans les prismes d'accretion sedimentaire: modélization analogique. Ph.D. Thesis, Université de Montpellier II.
Cerveny, V., Psencik, I., 1984. Documentation of Earthquake Algorithms. SEIS83 - Numerical modeling of seismic wave fields in 2-D laterally varying layered structures by the ray method. E.R.Engdahl edit., Report SE-35, Boulder, 36-40.
Chen, W., Chen, C., Nabelek, J., 1999. Present-day deformation of the Qaidam Basin with implications for intra-continental tectonics. Tectonophysics 305, 165–181.
Christensen, N.I., 1979. Compressional wave velocities in rocks at high temperatures and pressures, critical thermal gradients, and crustal low-velocity zones. Journal of Geophysical Research 84, 6849–6857.
Christensen, N.I., Mooney, W.D., 1995. Seismic velocity structure and composition of the continental crust: a global view. Journal of Geophysical Research 101, 9761–9788.
Chung, S.L., Chu, M.F., Zhang, Y.Q., Xie, Y.W., Lo, C.H., Lee, T.Y., Lan, C.Y., Li, X.H., Zhang, Q., Wang, Y.Z., 2005. Tibetan tectonic evolution inferred from spatial and temporal variations in post-collisional magmatism. Earth-Science Reviews 68, 73–196.
Dai, J., Wang, C., Hébert, R., Li, Y., Zhong, H., Guillaume, R., Bezard, R., Wei, Y., 2010. Late Devonian OIB alkaline gabbro in the Yarlung Zangbo Suture Zone: remnants of the Paleo-Tethys? Gondwana Research, doi:10.1016/j.gr.2010.05.015.
Deng, W.M., 1997. Cenozoic volcanism and lithosphere tectonic evolution in the northern Tibetan plateau, China. In: Li, Z.N., Qi, J.Z., Zhang, Z.C. (Eds.), Igneous Petrology. 30th International Geological Congress, vol. 15. Utrecht, The Netherlands Tokyo, Japan, pp. 3–12.
Elena, A.K., Brunel, M., Malavielle, J., 2003. Discovery of the Paleo-Tethys residual peridotites along the Anyemaqen–KunLun suture zone (North Tibet). Comptes Rendus Geoscience 335 (8), 709.
Fang, X., Yan, M., Van der Voo, R., Rea, D.K., Song, C., Parés, J.M., Gao, J., Nie, J., Shuang Dai, S., 2005. Late Cenozoic deformation and uplift of the NE Tibetan Plateau: evidence from high-resolution magnetostratigraphy of the Guide Basin, Qinghai Province, China. Geological Society of America Bulletin 117, 1208–1225.
Fliedner, M.M., Klemperer, S.L., 2000. Crustal structure transition from oceanic arc to continental arc, eastern Aleutian Islands and Alaska Peninsula. Earth and Planetary Science Letters 179, 567–579.
Fliedner, M.M., Klemperer, S.L., Christensen, N.I., 2000. Three-dimensional seismic model of the Sierra Nevada arc, California, and its implications for crustal and upper mantle composition. Journal of Geophysical Research 105, 10 899–10 921.
Fu, B.H., Awata, Y., 2007. Displacement and timing of left-lateral faulting in the Kunlun Fault Zone, northern Tibet, inferred geologic and geomorphic features. Journal of Asian Earth Sciences 29, 253–265.
Fu, X.G., Wang, J., Tan, F.W., Chen, M., Chen, W.B., 2010. The Late Triassic rift-related volcanic rocks from eastern Qiangtang, northern Tibet (China): age and tectonic implications. Gondwana Research 17, 135–144.
Galvé, A., Hirn, A., Jiang, M., Gallart, J., de Voogd, B., Lepine, J.C., Diaz, J., Wang, Y.X., Qian, H., 2002. Modes of raising northeastern Tibet probed by explosion seismology. Earth and Planetary Science Letters 203, 35–43.
Gao, Y., Wu, Z.-L., Liu, Z., Zhou, H.-L., 2000. Seismic source characteristics of nine strong earthquakes from 1988 to 1990 and earthquake activity since 1970 in the Sichuan–Qinghai–Xizang (Tibet) zone of China. Pure Applied Geophysics 157 (9), 1423–1443.
Guo, Z., Deng, J., Xu, Z., Mo, X., Luo, Z., 1998. Late Palaeozoic–Mesozoic intracontinental orogenic process and intermediate–acidic igneous rocks from the Eastern Kunlun mountains in north Tibet, northwestern China. Geoscience 12, 344–352 (in Chinese with English abstract).
Hirn, A., Nercessian, A., Sapin, M., Jobert, G., Xin, X.Z., Yuan, G.E., Yuan, L.D., Teng, J.W., 1984. Lhasa block and bordering sutures — A continuation of a 500 km Moho traverse through Tibet. Nature 307, 25–27.
Huang, Q., 1977. Basic tectonic framework of China continent. Acta Geologica Sinica 1977 (2), 27–44.
Jiang, C.F., Wang, Z.Q., Li, J.Y., 2000. Opening-Closing tectonics of the Central Orogenic Belt in China. Geological Publishing House, Beijing. 154 pp (in Chinese, with English abstract).
Jiang, M., Galvé, A., Hirn, A., de Voogd, B., Laigle, M., Su, H.P., Diaz, J., Lépine, J.C., Wang, Y.X., 2006. Crustal thickening and variations in architecture form the Qaidam basin to the Qang Tang (North-Central Tibetan Plateau) from wide-angle reflection seismology. Tectonophysics 412, 121–140.
Kao, H., Rui, G., Rau, R.J., Shi, D., Chen, R.Y., Guan, Y., Wu, F.T., 2001. Seismic image of the Tarim Basin and its collision with Tibet. Geology 29, 575–578.
Karplus, M., Zhao, W., Klemperer, S.L., Wu, Z., Mechie, J., Shi, D., Brown, L.D., Chen, C., 2010, Injection of Tibetan crust beneath South Qaidam Basin: evidence from INDEPTH IV wide-angle seismic data. Submitted to Journal of Geophysical Research-solid earth.
Kind, R., Yuan, X., Saul, J., Nelson, D., Sobolev, S.V., Mechie, J., Zhao, W., Kosarev, G., Ni, J., Achauer, U., Jiang, M., 2002. Seismic images of crust and upper mantle beneath Tibet: evidence for Eurasian Plate subduction. Science 298, 1219–1221.
Klemperer, S.L., 2006. Crustal flow in Tibet: geophysical evidence for the physical state of Tibetan lithosphere, and inferred patterns of active flow. In: Law, R.D., Searle, M.P., Godin, L. (Eds.), Channel flow, ductile extrusion and exhumation in continental collision zones, Geol. Soc. Lond. Special Publication, vol. 268, pp. 39–70.
Lerch, D.W., Klemperer, S.L., Glen, J.M.G., Ponce, D.A., Miller, E.L., Colgan, J.P., 2007. Crustal structure of the northwestern Basin and Range Province and its transition to unextended volcanic plateaus. Geochemistry Geophysics Geosystems 8 (2), Q02011, 21 pp., doi:10.1029/2006GC001429.

Li, Q.S., Gao, R., Lu, D.Y., Li, J.W., Fan, J.Y., Zhang, Z.Y., Liu, W., Li, Y.K., Yan, Q.R., Li, D.X., Wide Angle team, 2001. Tarim underthrust beneath western Kunlun: evidence from wide-angle seismic sounding. Journal of Asian Earth Sciences 18, 281–292.
Liang, C., Song, X., 2006. A low velocity belt beneath northern and eastern Tibetan Plateau from Pn tomography. Geophysical Research Letters 33, L22306, doi:10.1029/2006GL027926.
Liu, M.J., Mooney, W.D., Li, S.L., Okaya, N., Detweiler, S., 2006. Crustal structure of the northeastern margin of the Tibetan plateau from the Songpan-Ganzi terrane to the Ordos basin. Tectonophysics 420, 253–266.
Lutter, W.J., Nowack, R.L., 1990. Inversion for crustal structure using reflections from the PASSCAL Ouachita experiment. Journal of Geophysical Research 95, 4633–4646.
Lutter, W.J., Nowack, R.L., Braile, L., 1990. Seismic imaging of upper crustal structure using travel times from the PASSCAL Ouachita experiment. Journal of Geophysical Research 95, 4621–4631.
Makovsky, Y., Klemperer, S.L., Huang, L., Lu, D., Project INDEPTH Team, 1996. Structural elements of the southern Tethyan Himalaya crust from wide-angle seismic data. Tectonics 15, 997–1005.
Makovsky, Y., Klemperer, S., Ratschbacher, L., Alsdorf, D., 1999. Midcrust reflector on INDEPTH wide-angle profiles: an ophiolitic slab beneath the Indian–Asia suture in southern Tibet. Tectonics 18 (5), 793–808.
Mattauer, M., Malavieille, J., Calassou, S., Lancelot, J., Roger, F., Hao, Z.W., Xu, Z.Q., Hou, L.W., 1992. La chaîne triasique de Songpan–Garzê (Ouest Sechuan et est Tibet): une chaîne de plissement–décollement sur marge passive. Comptes Rendus de l'Académie des Sciences, Série II 314, 619–626.
Metcalfe, I., 2010. Tectonic framework and Phanerozoic evolution of Sundaland. Gondwana Research, doi:10.1016/j.gr.2010.02.016.
Metivier, F., Gaudemer, Y., Tapponnier, P., Meyer, B., 1998. Northeastward growth of the Tibet Plateau deduced from balanced reconstruction of two depositional areas: the Qaidam and Hexi Corridor basins, China. Tectonics 17, 823–842.
Meyer, B., Tapponnier, P., Bourjot, L., Metevier, F., Gaudemer, Y., Peltzer, G., Guo, S., Chen, Z., 1998. Crustal thickening in Gansu–Qinghai, lithospheric mantle subduction, and oblique, strike-slip controlled growth of the Tibet plateau. Geophysical Journal International 135, 1–47.
Molnar, P., England, P., Martinod, J., 1993. Mantle dynamics, uplift of the Tibetan plateau and the Indian Monsoon. Reviews of Geophysics 31, 357–396.
Mooney, W.D., Braile, L.W., 1989. The seismic structure of the continental crust and upper mantle of North America. In: Bally, A.W., Palmer, A.R. (Eds.), Geological Society of America, Boulder, Colorado, pp. 39–52.
Nie, S., Yin, A., Rowley, D.B., Jin, Y., 1994. Exhumation of the Dabie Shan ultra-high pressure rocks and accumulation of the Songpan–Ganzi flysch sequence, central China. Geology 22, 999–1002.
Owens, T.J., Zandt, G., 1997. Implications of crustal property variations for models of Tibetan plateau evolution. Nature 387, 37–43.
Pan, G.T., Ding, J., Yao, D.S., Wang, L.Q., 2004. Geological map of Qinghai-Tibet Plateau and adjacent region (scale: 1:1,500,000) Chengdu Institute of Geology and Mineral Resources, Geological Survey of China. Chengdu Cartographic Publishing House, Chengdu, China.
Panza, G.F., Raykova, R.B., 2008. Structure and rheology of lithosphere in Italy and surrounding. Terra Nova 20 (3), 194–199.
Pares, J.M., Van der Voo, R., Downs, W.R., Yan, M., Fang, X.M., 2003. Northeastward growth and uplift of the Tibetan Plateau: magnetostratigraphic insights from the Guide Basin. Journal of Geophysical Research 108 (B1), 2017, doi:10.1029/2001JB001349.
Pearce, J.A., Mei, H.J., 1988. Volcanic rocks of the 1985 Tibet geotraverse Lhasa to Golmud. The geological evolution of Tibet. Philosophical Transactions of the Royal Society of London 169–201.
Podvin, P., Lecomte, I., 1991. Finite difference computation of traveltimes in very contrasted velocity models: a massively parallel approach and its associated tools. Geophysical Journal International 105, 271–284.
Powell, C. McA, Conaghan, P.J., 1975. Tectonic models of the Tibetan plateau. Geology 3, 727–731.
Rao, R., Xu, J., Chen, Y., Zou, D., 1987. The Triassic System of the Qinaghai–Xizang Plateau. Geological Publishing House, Beijing. 239 pp.
Roger, F., Malavieille, J., Leloup, Ph. H., Calassou, S., Xu, Z., 2004. Timing of granite emplacement and cooling in the Songpan-Garze (eastern Tibetan Plateau) with tectonic implications. J. Asian Earth Sci. 22, 465–481.
Royden, L.H., Burchfiel, B.C., King, R.W., Wang, E., Chen, Z., Shen, F., Liu, Y., 1997. Surface Deformation and Lower Crustal Flow in Eastern Tibet. Science 276, 788–790.
Schneider, W.A.J., Ranzinger, K., Balch, A., Kruse, C., 1992. A dynamic programming approach to first arrival traveltime computation in media with arbitrarily distributed velocities. Geophysics 57, 39–50.
Shillington, D.J., Scott, C.L., Minshull, T.A., Edwards, R.A., Brown, P.J., White, N., 2009. An abrupt transition from magma-starved to magma-rich rifting in the eastern Black Sea. Geology 37, 7–10.
Takahashi, N., Kodaira, S., Klemperer, S.L., Tatsumi, Y., Kaneda, Y., Suyehiro, K., 2008. Crustal structure and evolution of the Mariana intra-oceanic island arc. Geology 35, 203–206.
Tapponnier, P., Meyer, B., Avouac, J., Gaudemer, Y., Peltzer, G., Guo, S., Xiang, H., Yin, K., Chen, Z., Cai, S., Dai, H., 1990. Active thrusting and folding in the Qilian Shan, and decoupling between upper crust and mantle in northeastern Tibet. Earth and Planetary Science letters 97, 382–403.
Tapponnier, P., Xu, Z., Roger, F., Meyer, B., Arnaud, N., Wittlinger, G., Yang, J., 2001. Oblique stepwise rise and growth of the Tibet plateau. Science 294, 1671–1677.
Teng, J.W., Xiong, S.B., Yin, Z.X., 1985. Structure of the crust and upper mantle pattern and velocity distribution characteristics in the northern region of the Himalayan mountain region. Journal of Physics of the Earth 33, 157–171.
Van der Woerd, J., Ryerson, F.J., Tapponnier, P., Meriaux, A.S., Gaudemer, Y., Meyer, B., Finkel, R.C., Caffee, M.W., Zhao, G.G., Xu, Z.Q., 2000. Uniform slip-rate along the Kunlun Fault: implications for seismic behaviour and large-scale tectonics. Geophysical Research Letters 27, 2353–2356.
Vergne, J., Wittlinger, G., Qiang, H., Tapponnier, P., Poupinet, G., Jiang, M., Herquel, G., Paul, A., 2002. Seismic evidence for stepwise thickening of the crust across the NE Tibetan plateau. Earth and Planetary Science Letters 203, 25–33.
Vidale, J.E., 1990. Finite-difference calculation of traveltimes in three dimensions. Geophysics 55, 521–526.
Wang, Y.B., Huang, J.C., Luo, M.S., Tian, J., Bai, Y.S., 1997. Paleo-ocean evolution of the southern eastern Kunlun orogenic belt during Hercy-Early Indosinian. Earth Science-Journal of China University of Geosciences 22, 369–372 (in Chinese, with English abstract).
Wang, Y.X., Mooney, W., Yuan, X.C., Okaya, N., in press. Crustal structure of the Northeastern Tibetan Plateau from the Southern Tarim basin to the Sichuan Basin. Journal of Geophysical Research.
Wang, Z.Q., Jiang, C.F., Yan, Q.R., Yan, Z., 2001a. Accretion and Collision Orogeneses in the West Kunlun Mountains, China. Gondwana Research 4, 843–844.
Wang, Z.Q., Jiang, C.F., Yan, Q.R., Yan, Z., 2001b. Accretion and Collision Orogeneses in the West Kunlun Mountains, China. Gondwana Research 4, 843–844.
Weislogel, A.L., 2008. Tectonostratigraphic and geochronologic constraints on evolution of the northeast Paleotethys from the Songpan-Ganzi Complex, central China. Tectonophysics 451, 331–345.
Wittlinger, G., Vergne, J., Tapponnier, P., Farra, V., Poupinet, G., Jiang, M., Su, H., Herquel, G., Paul, A., 2004. Teleseismic imaging of subducting lithosphere and Moho offsets beneath western Tibet. Earth and Planetary Science Letters 221, 117–130.
Wu, G., Xiao, X., Li, T., Cheng, Q., Cui, G., Cui, Z., Dong, X., Gao, R., Huang, H., Liu, X., Meng, L., Sheng, X., Yu, Q., 1993. Lithospheric structure and evolution of the Tibetan Plateau: the Yadong-Golmud Geoscience transect. Tectonophysics 219, 213–221.
Wyllie, M.R.J., Gregory, A.R., Gardner, L.W., 1956. Elastic wave velocities in heterogeneous and porous media. Geophysics 21, 41–70.
Xiao, W.J., Windley, B.F., Fang, A.M., Zhou, H., Yuan, C., Wang, Z.H., Hao, J., Hou, Q.L., Li, J.L., 2001. Palaeozoic-Early Mesozoic Accretionary Tectonics of the Western Kunlun Range, NW China. Gondwana Research 4, 826–827.
Xiao, W.J., Windley, B.F., Chen, H.L., Zhang, G.C., Li, J.L., 2002. Carboniferous-Triassic subduction and accretion in the western Kunlun, China: implications for the collisional and accretionary tectonics of the northern Tibetan plateau. Geology 30, 295–298.
Xu, Z.Q., Hou, L.W., Wang, Z.X., Fu, X.F., Huang, M.H., 1992. Orogenic Processes of the Songpan–Ganze Orogenic Belt of China. Geological Publishing House, Beijing. (in Chinese).
Yang, Z.Y., Chen, Y.Q., Wang, H.Z., 1986. The Geology of China. Clarendon, Oxford. 303 pp.
Yang, J.S., Robinson, P.T., Jing, C.F., Xu, Z.Q., 1996. Tectonophysics 215–231.
Ye, H.M., Li, X.H., Li, Z.X., Zhang, C.L., 2008. Age and origin of high Ba–Sr appinite–granites at the northwestern margin of the Tibet Plateau: Implications for early Paleozoic tectonic evolution of the Western Kunlun orogenic belt. Gondwana Research 13, 126–138.
Yin, A., Harrison, T.M., 2000. Geologic evolution of the Himalayan–Tibetan orogen. Annual Review of Earth and Planetary Sciences 28, 211–280.
Yuan, X.C., Hua, J.R., 1996. Geophysics Atlas of China. Geology Press, Beijing, pp. 135–144.
Zelt, C.A., 1999. Modelling strategies and model assessment for wide-angle seismic traveltime data. Geophysical Journal International 139, 183–204.
Zelt, C.A., Smith, R.B., 1992. Seismic traveltime inversion for 2-D crustal velocity structure. Geophysical Journal International 108, 16–34.
Zhang, K.J., 2001. Is the Songpan-Ganzi terrane (central China) really underlain by oceanic crust? Journal of the Geological Society of India 57, 223–230.
Zhang, Z.J., Klemperer, S.L., 2005. West-east variation in crustal thickness in northern Lhasa block, central Tibet, from deep seismic sounding data. Journal of Geophysical Research 110 (B09403), 14, doi:10.1029/2004JB003139.
Zhang, Z.J., Klemperer, S.L., 2010. Crustal structure of the Tethyan Himalaya, south Tibet: new constraints from old wide-angle seismic data. Geophysical Journal International 181, 1247–1260, doi:10.1111/j.1365-246X.2010.04578.x.
Zhang, Z.J., Wang, G.J., Sun, R.M., Teng, J.W., Yang, L.Q., Qin, Y.L., Chen, Y., Zhang, C.Y., Li, Y.K., Lu, D.Y., Zheng, H.S., 2003. P-wave velocity of the crust from Chayu, Xizang to Gonghe, Qinghai in the southeastern Tibet. IUGG Assembly, Japan.
Zhang, Z.J., Wang, Y., Chen, Y., Houseman, G.A., Tian, X., Wang, E., Teng, J., 2009. Crustal structure across Longmenshan fault belt from passive source seismic profiling. Geophysical Research letters 36, L17310, doi:10.1029/2009GL039580.
Zhang, C., Yang, D., Wang, H., Takahashi, Y., Ye, H., 2010a. Neoproterozoic mafic-ultramafic layered intrusion in Quruqtagh of northeastern Tarim Block, NW China: two phases of mafic igneous activity with different mantle resources. Gondwana Research, doi:10.1016/j.gr.2010.03.012.
Zhang, Z.J., Yuan, X.H., Chen, Y., Tian, X.B., Kind, R., Li, X.Q., Teng, J.W., 2010b. Seismic signature of the collision between the east Tibetan escape flow and the Sichuan Basin. Earth and Planetary Science Letters 292, 254–264.
Zhang, Z.J., Deng, Y.F., Teng, J.W., Wang, C.Y., Gao, R., Chen, Y., Fan, W.M., 2010c. An overview of the crustal structure of the Tibetan plateau after 35 years of deep seismic soundings. Journal of Asian Earth Sciences, doi:10.1016/j.jseaes.2010.03.010.
Zhao, W.L., Morgan, W., 1985. Uplift of Tibetan Plateau. Tectonics 4, 359–369.
Zhao, W.J., Mechie, J., Brown, L.D., Guo, J., Haines, S., Hearn, T., Klemperer, S.L., Ma, Y.S., Meissner, R., Nelson, K.D., Pananont, P., Rapine, R., Ross, A., Saul, J., 2001. Crustal structure of central Tibet as derived from Project INDEPTH wide-angle seismic data. Geophysical Journal International 145, 486–496.
Zhao, W.J., Brown, L., Wu, Z., Klemperer, S.L., Shi, D., Mechie, J., Su, H., Tilmann, F., Karplus, M.S., Makovsky, Y., 2008. Seismology Across the Northeastern Edge of the Tibetan Plateau. Eos. Transactions American Geophysical Union 89 (48), 487.
Zhu, L.P., Helmberger, L.V., 1998. Moho offset across the northern margin of Tibetan plateau. Science 281, 1170–1172.